



HAL
open science

Association of surface dielectric barrier discharge and photocatalysis in continuous reactor at pilot scale: butyraldehyde oxidation, by-products identification and ozone valorization

Sara Gharib-Abou Ghaida, Aymen Amine Assadi, Guillerme Costa, Abdelkrim Bouzaza, Dominique Wolbert

► To cite this version:

Sara Gharib-Abou Ghaida, Aymen Amine Assadi, Guillerme Costa, Abdelkrim Bouzaza, Dominique Wolbert. Association of surface dielectric barrier discharge and photocatalysis in continuous reactor at pilot scale: butyraldehyde oxidation, by-products identification and ozone valorization. *Chemical Engineering Journal*, 2016, 292, pp.276-283. 10.1016/j.cej.2016.02.029 . hal-01274114

HAL Id: hal-01274114

<https://hal-univ-rennes1.archives-ouvertes.fr/hal-01274114>

Submitted on 27 Apr 2016

HAL is a multi-disciplinary open access archive for the deposit and dissemination of scientific research documents, whether they are published or not. The documents may come from teaching and research institutions in France or abroad, or from public or private research centers.

L'archive ouverte pluridisciplinaire **HAL**, est destinée au dépôt et à la diffusion de documents scientifiques de niveau recherche, publiés ou non, émanant des établissements d'enseignement et de recherche français ou étrangers, des laboratoires publics ou privés.

1 **Association of surface dielectric barrier discharge and photocatalysis in**
2 **continuous reactor at pilot scale: butyraldehyde oxidation, by-products**
3 **identification and ozone valorization**

4 GHARIB-ABOU GHADA Sara, ASSADI Aymen Amine *, COSTA Guillaume, BOUZA
5 Abdelkrim, WOLBERT Dominique

6 Laboratoire Sciences Chimiques de Rennes - équipe Chimie et Ingénierie des Procédés, UMR 6226
7 CNRS, ENSCR -11, allée de Beaulieu, CS 508307-35708 Rennes, France.

8 * Corresponding author. Tel.: +33 2 23238092; fax: +33 2 23238120.

9 E-mail address: Aymen.assadi@ensc-rennes.fr (A. ASSADI).

10
11 **Abstract**

12 Coupling nonthermal plasma with other processes has been studied over the past few years
13 and promising results were obtained concerning VOCs removal for atmospheric pollution
14 control. In this work, butyraldehyde (BUTY) removal by a dielectric barrier discharge (DBD)
15 plasma coupled with different (photo) catalysts based on TiO₂ and MnO₂ was studied. DBD
16 plasma system and an immobilized TiO₂ and MnO₂ at different percentages are continually
17 and sequentially combined in order to decompose residual ozone. Indeed, different ways of
18 combination are listed. Effects of relative humidity and initial BUTY concentration on its
19 conversion rate and the distribution of byproducts were examined and discussed. Results with
20 pilot scale showed that combination of plasma and photocatalysis led to an enhancement of
21 BUTY abatement compared to the separate systems. When 100% of MnO₂ catalyst was
22 placed in the post discharge zone, the performance of sequential DBD/MnO₂ combined
23 system is improved in terms of decomposition and conversion rate of the pollutant. In the
24 same way, CO was reduced and CO₂ selectivity was significantly improved when compared
25 to the DBD plasma alone. Intermediate byproducts were identified and BUTY removal
26 pathways are suggested.

27 **Keywords**

28 Pilot scale, Sequential coupling processes, DBD plasma, photocatalysis, TiO₂/MnO₂
29 Catalysis.

1 **1. Introduction**

2
3 Volatile organic compounds (VOCs) constitute one of the most important family of chemicals
4 involved in atmospheric pollution, causing damage to environment and human health [1–3],
5 and need, consequently, to be eliminated. Nevertheless, gas effluents containing low VOCs
6 concentrations are not efficiently treated by conventional industrial processes, for which high
7 power is usually required (i.e. thermal oxidation or catalytic oxidation) [4]. Thus, alternative
8 solutions were investigated over the years, among which nonthermal plasma (NTP) is proved
9 to be an effective technology for the treatment of such effluents with low concentrations
10 particularly [4, 5]. Dielectric barrier discharge (DBD) is commonly used to create NTP, by
11 applying electrical energy between the two electrodes of the reactor, where at least one of
12 which is covered with dielectric material [6], in order to create high energy electrons (1–10
13 eV) [5], under moderate conditions (i.e. room temperature and atmospheric pressure)[1, 7].
14 These electrons are more likely to collide with gas molecules other than the pollutants since
15 their concentrations are low. This results in the production of reactive species such as ions,
16 free radicals and excited species able to react with the pollutants and oxidize them into less
17 harmful compounds [4, 8, 9]. However, debate is still widely open concerning the merits and
18 demerits of this technology. On one hand, nonthermal plasma permits the oxidation of VOCs
19 at relatively low energy cost [2, 4], but, on the other hand, it has many disadvantages such as
20 low energy efficiencies, poor selectivity to CO₂ even when high conversion rate is reached,
21 and undesirable byproducts formation (e.g. NO_x, ozone, etc.) [5, 9, 10]. Among promising
22 techniques to overcome these limitations, combining plasma NTP with suitable heterogeneous
23 catalysts has been proved to improve the efficiency of VOCs abatement [4], as a synergy
24 effect between NTP and catalytic action is greatly expected [1]. Two configurations of
25 plasma-catalysis are widely used so far: single-stage (also called plasma-driven catalysis PDC
26 or in-plasma catalysis IPC), where catalysts are placed directly in the discharge zone, and
27 two-stage (plasma-enhanced catalysis PEC or post-plasma catalysis PPC), where catalysts are
28 placed downstream the reactor [4, 11].

29 The aim of the present work is to study the decomposition of butyraldehyde at pilot scale
30 using surface dielectric barrier discharge (SDBD) and different (photo) catalysts made of
31 titanium dioxide (TiO₂), manganese dioxide (MnO₂), and a mixture of both, in order to
32 determine their catalytic efficiency when coupled with plasma NTP. Moreover, the novelty of
33 this study is the investigation of different configurations in order to optimize and valorize the

1 residual ozone. Finally, butyraldehyde reaction by-products are identified and a reactional
2 pathway is suggested.

3 **2. Material and methods**

4 **2.1. Pilot-scale reactor**

5
6 The reactor consists of a glass chamber (length $L = 1000\text{mm}$, width $l = 135\text{mm}$ and height H
7 $= 135\text{ mm}$), inside of which two glass plates acting as the dielectric media hold, on the inner
8 side, the catalytic media and high voltage grids (stainless steel, rectangular shaped and 2 mm
9 thickness) and on the outer side, a copper plate forming the outer electrode (1 mm thick and
10 800mm in length). The electrodes are connected to a generator and an amplifier. A coil of
11 capacitors with a total capacity of 2.5 nF is placed between the copper electrode and the
12 connection to ground in order to collect the charges created in the reactor. These two plates
13 are placed one opposite the other at an adjustable distance (Figure 1).

14 To generate the plasma, high voltage is applied to the reactor. The applied voltage is
15 generated by a generator (BFi OPTILAS) as a sinusoidal waveform up to 10V and then
16 amplified by an amplifier (TREK 30/40) to achieve 30 kV. The DBD plasma is obtained by
17 subjecting the electrodes to a sinusoidal high voltage ranging from 0 to 30 kV at a frequency
18 of 50 to 200Hz. The applied voltage (U_{app}) and the voltage across the capacitors (U_{m}) are
19 measured by two probes Optilas connected to a digital oscilloscope (Lecroy wave Surfer 24
20 Xs 200 MHz).

21

22 **Figure 1. Sectional drawing and Schema of NTP coupled with catalysis in planar** 23 **reactor.**

24

25 The reactor can be used also as a photocatalytic reactor and as a plasma DBD-photocatalytic
26 reactor. Eight lamps (Philips PL-S 9W / 10 / 4P) continuously emitting between 300 and 460
27 nm with a maximum at 365 nm are placed equidistant from each other in the inter-plate space.
28 The photocatalytic medium is interposed between the stainless steel grid electrode and the
29 dielectric barrier in the plasma active area. It should be noted that the plasma does not activate
30 the photocatalyst in the reactor. The UV lamps arranged in the reactor, permit the activation

1 of the photocatalyst. Two configurations (continuous and sequential combined system) were
2 tested (Figure 1).

3

4 **2.2. Catalysts**

5 The supported material has been provided by Ahlstrom Research and Services [12]. It is
6 further named Glass Fiber Tissue (GFT) containing colloidal silica, a variable percentage of
7 titanium dioxide and manganese dioxide nanoparticles and inorganic fibers. In fact, titanium
8 dioxide or manganese dioxides have been deposited on inorganic fibers by impregnation using
9 an industrial-size press (Figure 2). A dry mixture of 50 wt% colloidal silica and different wt%
10 of titanium dioxide nanoparticles (PC500 Millennium) and manganese dioxide is suspended
11 in pure water. In order to ensure the deposition of 13 g/m² of dry TiO₂ and/or MnO₂ on fiber
12 support, the suspension is composed of 40% of dry powder and 60% of pure water. PC500
13 TiO₂ nanoparticles are 5–10 nm in diameter and are of pure anatase form. The specific area of
14 TiO₂ nanoparticles is 300 m²/g. The specific area of MnO₂ nanoparticles is 377 m²/g. The
15 coating process consists in impregnating fibers using industrial size press. The press is
16 employed to impregnate fibers with the suspension; then, they are dried (Figure 2). Material
17 preparation has been performed by Ahlstrom Research and Services.

18

19 **Figure 2. Diagram of the impregnation technique for GFT synthesis "size press"**

20

21 Three catalysts media were produced: GFT with 100 % TiO₂, GFT with 100% MnO₂ and
22 GFT with 25% MnO₂ + 75% TiO₂.

23

24 **2.3. Polluted air flow generation**

25

26 Dry air flow is obtained by an air compressing system.

27 Butyraldehyde, in liquid state, is directly injected in the flow through a syringe/pump system
28 and the pollutant feed is done continuously through a septum. A heating tape is wrapped
29 around the pipe at the injection zone to ensure good evaporation of the pollutant.
30 Homogenization of the air/pollutant mixture is ensured by a static mixer placed between the
31 syringe/pump system and the reactor. The experiment is carried out at room temperature and

1 atmospheric pressure. The temperature and relative humidity are measured by a TESTO
2 sensor.

3 The main air flow can be generated by the internal network of compressed air when dry air is
4 needed (5% relative humidity) or by using ambient air when working at a higher flow rate.

5 The compressed air network enables moisture to be controlled by varying the flow in a packed
6 air-water countercurrent column. Thus, it is possible to obtain a range of relative humidity
7 (RH) from 5 to 90%. The entering air flow is measured in real time by a mass flow meter
8 (Bronkhorst In-Flow) calibrated normal cubic meter per hour on the range 0-20 Nm³.h⁻¹.

9

10 **2.4. Pollutant and by-products analysis**

11

12 The pollutant analysis can only start once the air flow in the reactor reaches equilibrium. In
13 other words, a certain time is required after the pollutant is injected in the air flow crossing
14 the reactor, so that its concentration stabilizes. Once the outlet concentration is stabilized and
15 the catalyst is loaded, plasma DBD is generated and oxidation begins. At this point, samples
16 for pollutant analysis can be taken. Two openings with septum permit taking gas samples at
17 the entrance and exit of the reactor. Analysis of butyraldehyde is performed using a gas
18 chromatography coupled to a Fisons flame ionization detector (GC-FID). A column
19 Chrompack FFAP-CB (25m in length and 0.32mm outer diameter) corresponding to the
20 volatile fatty acids is used. Nitrogen is the carrier gas and constitutes the mobile phase. All
21 injections are done manually with a syringe of 1 ml and were repeated at least three times.

22 The byproducts generated during the DBD plasma oxidation of butyraldehyde are identified
23 and evaluated by Gas Chromatograph-Mass spectrometer (GC-MS) (Perkin Elmer Clarus
24 500) equipped with an infrared (IR) detector. The temperature conditions in the oven, the
25 injection chamber and the detector are, respectively, 100, 120 and 200°C. Due to their low
26 concentrations, byproducts are concentrated in a Carbotrap (25ml) then removed by thermal
27 desorption unit coupled with GC-MS [13].

28

29 **2.5. CO₂, CO and O₃ analysis**

30

31 CO₂ outlet concentrations are measured by a Fourier Transform Infrared (FTIR)
32 spectrophotometer brand Environment SA (Cosma Beryl® reference 100, Cosma® Igny,
33 France). The measurement accuracy is about 5%[13]. CO outlet concentrations are measured

1 by a NO/CO_ZRE gas analyzer. CO₂ and CO selectivity's are calculated according to the
2 following equations:

3

$$4 \quad S_{CO_2} = \frac{\Delta CO_2}{n_{(C|COV)}([COV]_0 - [COV]_s)} \quad (1)$$

$$5 \quad S_{CO} = \frac{\Delta CO}{n_{(C|COV)}([COV]_0 - [COV]_s)} \quad (2)$$

6

7 where [COV]₀ and [COV]_s are the inlet and outlet concentrations of BUTY respectively
8 (ppmv), n_(C|COV) is the number of the stoichiometric coefficient of the removal reaction. In our
9 case n is equal to 4.

10 A standard iodometric titration method is used to estimate the concentration of the ozone
11 formed during oxidation reactions by DBD plasma. Thus, at the reactor exit, a constant air
12 flow of 285 L.h⁻¹ is bubbled in a potassium iodide (KI) solution at 10⁻²M. I⁻ is oxidized into I₂
13 and thus gives a yellow solution. After, a standard iodometric titration method is used to
14 estimate the downstream ozone formation [13].

15

16 3. Results and discussion

17 To follow the degradation of butyraldehyde, two parameters were selected:

18 Conversion rate (CR), which was calculated as follow:

$$19 \quad CR (\%) = \frac{C_{in} - C_{out}}{C_{in}} \times 100 \quad (3)$$

20 Elimination Capacity (EC) which was estimated according to the equation:

$$21 \quad EC (mg/g.h) = \frac{C_{in} - C_{out}}{m_{TiO_2}} \times Q_{air} \quad (4)$$

22 Where C_{in} and C_{out} are the inlet and the outlet BUTY concentrations (mg.m⁻³), respectively.
23 m_{TiO₂} is the amount of catalyst deposited on glass fiber tissue.

24 Depending on the need, one or the other will be used for expressing the results obtained
25 during experiments.

26 3.1. Butyraldehyde oxidation: GFT with 100 % of TiO₂

27

1 We started our investigations by studying BUTY elimination by photocatalysis (UV/TiO₂)
2 and plasma DBD separately, then by coupling both technologies.

3 Figure (3) shows variation of the elimination capacity (EC) of butyraldehyde by
4 photocatalysis versus air flow rate and BUTY inlet concentration. On figure (4) the influence
5 of relative humidity (RH) is represented. It can be noted that butyraldehyde EC increases
6 when air flow rate and inlet pollutant concentration are increased. Knowing that
7 photocatalysis reaction is often assimilated to a pseudo-first order reaction, this means that a
8 greater flow of pollutant (due to the increased air flow rate or inlet concentration) naturally
9 induces an increase in the degradation kinetics [13–15]. Of course, for a constant amount of
10 catalyst, the percentage of degradation and mineralization will decrease when these operating
11 parameters increase.

12

13 **Figure 3. Variation of EC with inlet concentration at different flow rates (SE = 17 J.L⁻¹,**
14 **T = 20°C, RH = 5%, I = 20 W.m⁻²)**

15

16 The EC also varies with relative humidity and is optimal when approaching 25-30% for all
17 pollutant inlet concentrations tested. However, it is more visible for high inlet concentrations
18 (120 and 160 mg/Nm³). When RH exceeds a certain threshold, butyraldehyde EC decreases
19 remarkably.

20 In fact, RH has two opposite effects in photocatalysis alone. Initially, the presence of water
21 molecules in the air improves the EC of BUTY due to the dissociation of H₂O, forming new
22 reactive species (H[•] and HO[•]). Secondly, when RH rises too much, a competition effect
23 between the pollutant and water molecules for the active sites on the photocatalyst surface
24 predominates, diminishing consequently EC [12, 16].

25

26 **Figure 4. Variation of EC with RH at different inlet concentrations (SE = 17 J.L⁻¹, Q_{air}=**
27 **2 m³.h⁻¹, I = 20W.m⁻²)**

28

29 Figure 5 shows BUTY behavior when it is oxidized by plasma DBD alone or by coupling
30 (UV/TiO₂/DBD) in function of injected energy.

1 BUTY abatement is significantly better when coupling processes than with Photocatalysis or
2 DBD alone, whatever the injected energy, air flow rate or inlet pollutant concentration are.
3 With DBD alone, we note that BUTY conversion rate increases with the increase of injected
4 energy into the reactor (figure 5). This is due to an increase in the amount of radicals and
5 atomic oxygen produced. Indeed, the increase of the applied voltage in the reactor increases
6 the degree of ionization, and consequently the amount of reactive species produced. The
7 probability that the pollutant is attacked by radicals or electrons is higher [12].

8 Figure 5 also compares BUTY behavior when oxidized by photocatalysis and plasma DBD
9 separately, to its oxidation behavior due to coupling photocatalysis/plasma DBD versus RH
10 variation for a given injected energy.

11

12 **Figure 5. Variation of conversion rate with relative humidity vs. different processes**
13 **using GFT with 100% TiO₂ ($Q_{\text{air}} = 2 \text{ Nm}^3 \cdot \text{h}^{-1}$, $[\text{C}_4\text{H}_8\text{O}] = 80 \text{ mg} \cdot \text{Nm}^{-3}$, $E_{\text{inj}} = 17 \text{ J} \cdot \text{L}^{-1}$, RH**
14 **= 5-7%, T = 18-20°C)**

15

16 Clearly, BUTY removal is from 3 to 10% higher when coupling processes than using
17 photocatalysis or plasma separately. From the graphic above (Figure 5), the CR increases and
18 then drops. In fact, when RH increases, the competitive effect towards the active sites of
19 water and the consumption of actives species of plasma becomes predominant and thus the
20 CR decreases. We note an optimum at around 30% of RH. In our case the values of CR are
21 29.97%, 34.34% and 70.76% with photocatalysis, DBD and coupling respectively. In
22 addition, it must be pointed that coupling photocatalysis with DBD helps maintaining a
23 relatively high CR of butyraldehyde. For example, for RH = 80%, coupling insures a CR
24 equal to ~63%, while CR with photocatalysis and DBD does not exceed 23.05 and 27.47%
25 respectively.

26 This synergistic effect is observed under different experimental conditions. These
27 observations are similar to those obtained by several groups of researchers [14, 15, 17, 19].

28

29 **3.2. Intermediates identification**

1
2
3
4
5
6
7
8
9
10
11
12
13
14
15
16
17
18
19
20
21
22
23
24
25
26

We wanted to follow closely the degradation of butyraldehyde, so we decided to identify the degradation by-products by gas chromatography coupled to mass spectrometry (GC-MS).

Three samples were taken for butyraldehyde after each treatment process. Analyses of outlet unpolluted air flow composition after its treatment with each of the three processes have also been made in order to suppress any doubt while identifying butyraldehyde intermediates. The results are shown in figure 6.

Figure 6. By-products identified by GC-MS following butyraldehyde oxidation by the combined system

Compounds present in the outlet air were detected by GC-MS. Regarding butyraldehyde as pure substance and its oxidation by combined system; the detected degradation by-products were acetone (1), ethyl acetate (2), acetic acid (3), propionic acid (4) and butyric acid (5). Butyraldehyde is also detected at the exit of the reactor at 32.6 ppm. The same intermediates as in combined system were detected when plasma was used alone.

These results are comparable to those obtained by Ye et al. (2006) [19], where they were able to detect, after treatment by photocatalysis, the presence of acetic, propionic, and butyric acids, but in liquid phase. They detected other compounds in gas phase: propionaldehyde and acetaldehyde.

Since different oxidation mechanisms occur when plasma treatment is on, we suggest the following reactional mechanism for butyraldehyde degradation (Figure 7), where ethyl acetate and butyric acid derive directly from butyraldehyde and could dissociate into acetic acid, acetone and propionic acid (all detected with GC-MS), respectively, according to the represented reaction pathway.

1

2 **Figure 7. Suggested reaction scheme of BUTY oxidation by combination of GFT with**
3 **100% TiO₂ and DBD**

4

5 **3.3. CO and CO₂ selectivity, and ozone formation**

6

7 Figure 8 shows that photocatalysis is the most selective to CO₂ among the three processes
8 tested. We also note that introducing the photocatalyst (TiO₂) in the plasma can improve the
9 selectivity to CO₂. The production of CO is generally low and its concentration rarely exceed
10 10%. As for ozone, huge amounts are produced with plasma alone and with coupled
11 processes.

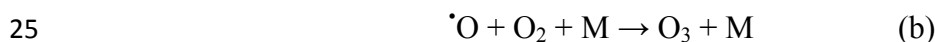
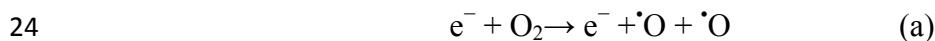
12 However, we also notice that for the same injected energy (12.8 J.L⁻¹), coupling ensures a
13 higher BUTY conversion rate while decreasing generated O₃ quantity. This behavior could be
14 explained by the fact that O₃ is decomposed in the presence of external UV light to the planar
15 reactor [16].

16

17 **Figure 8. CO₂ and CO selectivity's, and removal rate of oxidized butyraldehyde by**
18 **photocatalysis, plasma DBD and combined system (Q_{air} = 2 Nm³.h⁻¹, [C₄H₈O] = 80**
19 **mg.Nm⁻³, E_{inj} = 12.8 J.L⁻¹, RH = 5-7%, T = 18-20°C).**

20 **4. Effect of adding MnO₂ catalysis: continuous and sequential configurations**

21 Ozone is known to be an inevitable by-product of plasma. Interactions between highly
22 energetic electrons and molecular oxygen produce atomic oxygen. This latter interacts then
23 with molecular oxygen in the bulk gas to form ozone as follows [20]:



26 where M is a third body for discharging excess energy of the reaction, which can be N₂, O₂ or
27 a surface.

1 Although coupling DBD/photocatalysis processes reduces ozone generation like we discussed
2 previously, the concentrations emitted remain high (about some dozens of ppm) and
3 dangerously threatening human health. In fact, this oxidizing gas, even at relatively low
4 concentrations, is capable of damaging bronchiolar and alveolar cells and interacting with
5 some receptors and some protein molecules, lipids or certain enzymes [21]. Short-term
6 inhalation of ozone at concentrations that occur in urban environment causes acute conduit
7 artery vasoconstriction [22]. Due to its dangerous effects, it would be more benefic to
8 minimize its generation to avoid forming intermediate products that may be more toxic than
9 the original pollutant.

10 A second aim of the present study is, consequently, to minimize as much as possible and
11 valorize ozone production by implying it in the decomposition of pollutants. Thus, a series of
12 experiments was carried out under plasma, by testing different catalysts compositions and
13 their positions in the reactor.

14

15 **4.1. Continuous configurations (plasma and catalysis *in-situ*)**

16 In our tentative for reducing ozone emissions by the DBD process, a series of BUTY
17 oxidation experiments was carried out by testing different catalyst media. Three media was
18 tested, TiO₂ as a photocatalyst for VOCs removal [12–15, 17, 24–26], MnO₂ for ozone
19 degradation [26] and the combination of TiO₂/MnO₂ to enhance catalytic activity [27].

20

21 Figure 9 shows the influence of each catalyst mentioned above in butyraldehyde removal and
22 ozone formation.

23

24

25 **Figure 9. Effect of catalyst composition on BUTY conversion rate and the amount of**
26 **formed ozone by plasma-catalytic monobloc system (IPC) ($Q_{\text{air}} = 4 \text{ Nm}^{-3} \cdot \text{h}^{-1}$, $[\text{C}_4\text{H}_8\text{O}] =$**
27 **$50 \text{ mg} \cdot \text{Nm}^{-3}$, $E_{\text{inj}} = 12.96 \text{ J} \cdot \text{L}^{-1}$, $\text{RH} = 5\text{-}7 \%$, $T = 18\text{-}20^\circ\text{C}$)**

28

1 We note that MnO₂ alone is very reactive when activated by DBD alone. Compared to TiO₂
2 alone or DBD alone, it improves butyraldehyde abatement by a factor of 1.9, but surprisingly,
3 it increases also ozone production by a factor of 2.1. Probably this is due to the fact that the
4 presence of MnO₂ in the discharge zone may affect the discharge characteristics: an increase
5 in the production of active species [28] could have helped reducing the amount of consumed
6 ozone for butyraldehyde oxidation. Indeed, Ozone is created from atomic oxygen in a reaction
7 to three bodies according to reaction (b). When introducing the fibers into the plasma zone, it
8 expands the solid surface in contact with the plasma. This increases the probability that
9 oxygen enhances with third body for producing of ozone. Presumably oxygen atoms are
10 adsorbed on the surface and react with O₂. Accordingly, the ozone concentration increases
11 [30-32].

12 When hybridized with TiO₂, it reduces the generation of ozone by a factor of 7.2, but on the
13 other hand, it decreases by a factor of 1.7 butyraldehyde removal compared to MnO₂ alone. In
14 a first conclusion, we can note that hybrid catalyst seems to have the highest ozone removal
15 rate. However, since optimization of the reactor performance is our main objective, it would
16 be idealistic if we can achieve a highest removal rate with the lowest ozone generation. The
17 combined catalyst (75% TiO₂ + 25% MnO₂) permits to have the lowest ozone outlet
18 concentration when placed in the discharge zone, but it decreases pollutant removal rate by
19 almost the half. Thus, further investigation was conducted in order to study the reasons behind
20 this decrease in BUTY conversion rate. Experiments with UV/TiO₂, UV/MnO₂ and
21 UV/TiO₂/MnO₂ were performed (Figure 10). CR of butyraldehyde was compared to that
22 obtained with DBD/TiO₂-and/or-MnO₂ (Figure 9).

23

24 **Figure 10. Comparison of the photocatalytic performance of different media for BUTY**
25 **oxidation ($Q_{\text{air}} = 4 \text{ Nm}^{-3} \cdot \text{h}^{-1}$, $[\text{C}_4\text{H}_8\text{O}] = 50 \text{ mg} \cdot \text{Nm}^{-3}$, $\text{RH} = 5\text{-}7 \%$, $\text{T} = 18\text{-}20^\circ\text{C}$)**

26

27 Based on the obtained results, we note that the presence of MnO₂ seems to completely inhibit
28 the photocatalytic activity of TiO₂. A clear explanation for this finding has not been
29 established yet. However, some researchers working on the photocatalytic activity of TiO₂
30 combined with MnO₂ in liquid phase have found similar results [27, 29]. They admit that the
31 photocatalytic activity of TiO₂ under UV irradiation decreases when its surface is modified by
32 MnO₂ particles. These particles affect O₂ reduction. This leads to a decrease of UV radiations

1 and therefore their absorption by TiO_2 [30]. Heterojunctions formation between MnO_2 and
2 TiO_2 particles seems responsible for altering the chemical status of Ti^{4+} and O^{2-} sites in the
3 crystalline phase of TiO_2 [29]. This poisoning effect of TiO_2 by MnO_2 might be present in the
4 gas phase and could explain our results.

5

6 **4.2. Sequential combinations**

7

8 Since MnO_2 placed in the discharge zone was not efficient for reducing ozone generation by
9 DBD process, a second series of experiments was carried out, where MnO_2 is placed
10 downstream of the discharge zone. Reactor was in PPC configuration. Samples were taken
11 from the middle zone (Part I) and the exit of the reactor (Part II), i.e. before and after contact
12 with catalyst surface. Results obtained showed a huge reduction in ozone emissions along
13 with improvement in butyraldehyde CR (Figure 11). This observation suggests that ozone
14 produced in the discharge zone is dissociated on MnO_2 surface, generating more reactive
15 species contributing to BUTY oxidation [31].

16 Relative humidity, when increased, enhances ozone reduction significantly, but not BUTY
17 oxidation, CR decreases slightly (Figure 11). However, this increase in ozone reduction is not
18 clearly seen when inlet air flow rate is increased from 2 to 4 $\text{Nm}^3 \cdot \text{h}^{-1}$ (results not shown). This
19 could be due to the short residence time of butyraldehyde in the reactor. Thus, working with a
20 packed-bed of MnO_2 beads, instead of GFT, which could provide an increased contact of
21 BUTY with the catalyst surface, might be a better alternative.

22

23 **Figure 5. Effect of RH on BUTY conversion rate and ozone formation in PPC for the**
24 **same BUTY inlet concentration ($Q_{\text{air}} = 2 \text{ Nm}^3 \cdot \text{h}^{-1}$, $[\text{C}_4\text{H}_8\text{O}] = 50 \text{ mg} \cdot \text{Nm}^{-3}$, $E_{\text{inj}} =$**
25 **$12.96 \text{ J} \cdot \text{L}^{-1}$, $T = 18\text{-}20^\circ\text{C}$) On the left:, RH = 5-7 %, On the right: RH = 55 %.**

26

27 **5. Conclusions**

28

1 As a conclusion, we can note firstly that plasma/photocatalysis combination with UV light
2 provides better performance concerning Buty degradation. Secondly, UV/DBD/TiO₂
3 configuration results in a slight ozone reduction, an increase in CO₂ selectivity and a
4 synergistic effect was observed.

5 Influence of MnO₂ and MnO₂/TiO₂ media was also studied. When using DBD/MnO₂
6 combination with no external UV light, a better butyraldehyde oxidation in IPC configuration
7 was obtained but huge amounts of ozone was produced. Under PPC configuration, lower
8 ozone amounts but also lower butyraldehyde decomposition were obtained.

9 It seems that PPC configuration using MnO₂ catalyst without external UV light could be the
10 best compromise between good butyraldehyde decomposition and low ozone production.
11 Further optimization of the process is still required in order to obtain the same promising
12 results for higher air flow rates.

13

14 **6. Acknowledgments:**

15

16 This work is supported by the French National Research Agency (ANR). Alexander
17 Vorontsov (Boreskov Institute of Catalysis, Russia) is gratefully acknowledged for
18 highlighting discussions.

19

20

21

22

23

24

25

26

27

28

29

30

31

32

1
2
3
4
5
6
7
8
9
10
11
12
13
14
15
16
17
18
19
20
21
22
23
24
25
26
27
28
29
30
31
32
33
34
35
36
37
38

7. References:

- [1] J. Karuppiah, E. L. Reddy, P. M. Kumar, B. Ramaraju, R. Karvembu, and C. Subrahmanyam, "Abatement of mixture of volatile organic compounds (VOCs) in a catalytic non-thermal plasma reactor," *J. Hazard. Mater.*, vol. 237–238, pp. 283–289, 2012.
- [2] H. T. Quoc An, T. Pham Huu, T. Le Van, J. M. Cormier, and a. Khacef, "Application of atmospheric non thermal plasma-catalysis hybrid system for air pollution control: Toluene removal," *Catal. Today*, vol. 176, no. 1, pp. 474–477, 2011.
- [3] C. Subrahmanyam, "Catalytic non-thermal plasma reactor for total oxidation of volatile organic compounds," *Indian J. Chem.*, vol. 48, no. August, pp. 1062–1068, 2009.
- [4] J. Jarrige and P. Vervisch, "Plasma-enhanced catalysis of propane and isopropyl alcohol at ambient temperature on a MnO₂-based catalyst," *Appl. Catal. B Environ.*, vol. 90, no. 1–2, pp. 74–82, 2009.
- [5] Y. Guo, D. Ye, K. Chen, J. He, and W. Chen, "Toluene decomposition using a wire-plate dielectric barrier discharge reactor with manganese oxide catalyst in situ," vol. 245, pp. 93–100, 2006.
- [6] X. Tang, F. Gao, J. Wang, H. Yi, S. Zhao, B. Zhang, Y. Zuo, and Z. Wang, "Comparative Study between Single- and Double-Dielectric Barrier Discharge Reactor for Nitric Oxide Removal," pp. 6197–6203, 2014.

- 1
- 2 [7] H. Kim, Y. Teramoto, N. Negishi, and A. Ogata, “nonthermal plasma and catalyst : A
3 review,” *Catal. Today*, 2015.
4
- 5 [8] S. Delagrangue, L. Pinard, and J. Tatiboue, “Combination of a non-thermal plasma and a
6 catalyst for toluene removal from air : Manganese based oxide catalysts,” vol. 68, pp.
7 92–98, 2006.
8
- 9 [9] A. Pollution, C. Part, E. Marotta, A. Callea, and M. Rea, “DC Corona Electric
10 Discharges for Air Pollution Control. Part 1. Efficiency and Products of Hydrocarbon
11 Processing,” vol. 41, no. 16, pp. 5862–5868, 2007.
12
- 13 [10] U. Roland, F. Holzer, and F. D. Kopinke, “Combination of non-thermal plasma and
14 heterogeneous catalysis for oxidation of volatile organic compounds: Part 2. Ozone
15 decomposition and deactivation of γ -Al₂O₃,” *Appl. Catal. B Environ.*, vol. 58, no. 3–
16 4, pp. 217–226, 2005.
17
- 18 [11] G. Xiao, W. Xu, R. Wu, M. Ni, C. Du, X. Gao, Z. Luo, and K. Cen, *Non-thermal
19 plasmas for VOCs abatement*, vol. 34, no. 5. 2014.
20
- 21 [12] J. Palau, a. a. Assadi, J. M. Penya-roja, a. Bouzaza, D. Wolbert, and V. Martínez-
22 Soria, “Isovaleraldehyde degradation using UV photocatalytic and dielectric barrier
23 discharge reactors, and their combinations,” *J. Photochem. Photobiol. A Chem.*, vol.
24 299, pp. 110–117, 2015.
25
- 26 [13] A. A. Assadi, A. Bouzaza, M. Lemasle, and D. Wolbert, “Removal of trimethylamine
27 and isovaleric acid from gas streams in a continuous flow surface discharge plasma
28 reactor,” *Chem. Eng. Res. Des.*, pp. 1–12, 2014.
29
- 30 [14] A. A. Assadi, A. Bouzaza, and D. Wolbert, “Photocatalytic oxidation of
31 trimethylamine and isovaleraldehyde in an annular reactor: Influence of the mass
32 transfer and the relative humidity,” *J. Photochem. Photobiol. A Chem.*, vol. 236, pp.
33 61–69, 2012.
34
- 35 [15] A. A. Assadi, J. Palau, A. Bouzaza, J. Penya-Roja, V. Martinez-Soriac, and D.
36 Wolbert, “Abatement of 3-methylbutanal and trimethylamine with combined plasma
37 and photocatalysis in a continuous planar reactor,” *J. Photochem. Photobiol. A Chem.*,
38 vol. 282, pp. 1–8, 2014.
39
- 40 [16] A. A. Assadi, A. Bouzaza, S. Merabet, and D. Wolbert, “Modeling and simulation of
41 VOCs removal by nonthermal plasma discharge with photocatalysis in a continuous
42 reactor: Synergetic effect and mass transfer,” *Chem. Eng. J.*, vol. 258, pp. 119–127,
43 2014.

- 1
- 2 [17] Y. Guo, X. Liao, J. He, W. Ou, and D. Ye, "Effect of manganese oxide catalyst on the
3 dielectric barrier discharge decomposition of toluene," *Catal. Today*, vol. 153, no. 3–4,
4 pp. 176–183, 2010.
5
- 6 [18] A. V Vorontsov, M. N. Lyulyukin, and A. S. Besov, "Abatement of air pollutants in
7 combined plasma and photocatalytic systems," 2011.
8
- 9 [19] X. Ye, D. Chen, J. Gossage, and K. Li, "Photocatalytic oxidation of aldehydes:
10 Byproduct identification and reaction pathway," *J. Photochem. Photobiol. A Chem.*,
11 vol. 183, no. 1–2, pp. 35–40, 2006.
12
- 13 [20] R. Atkinson, D. L. Baulch, R. a. Cox, J. N. Crowley, R. F. Hampson, R. G. Hynes, M.
14 E. Jenkin, M. J. Rossi, J. Troe, and T. J. Wallington, "Evaluated kinetic and
15 photochemical data for atmospheric chemistry: Volume IV – gas phase
16 reactions of organic halogen species," *Atmos. Chem. Phys. Discuss.*, vol. 7, no. 6, pp.
17 16349–17067, 2007.
18
- 19 [21] L. Pascal, "Effets à court terme de la pollution atmosphérique sur la mortalité," *Revue*
20 *Française d'Allergologie*, vol. 49, no. 6. pp. 466–476, 2009.
21
- 22 [22] R. D. Brook, J. R. Brook, B. Urch, R. Vincent, S. Rajagopalan, and F. Silverman,
23 "Inhalation of fine particulate air pollution and ozone causes acute arterial
24 vasoconstriction in healthy adults," *Circulation*, vol. 105, no. 13, pp. 1534–1536, 2002.
25
- 26 [23] A. A. Assadi, A. Bouzaza, C. Vallet, and D. Wolbert, "Use of DBD plasma,
27 photocatalysis, and combined DBD plasma/photocatalysis in a continuous annular
28 reactor for isovaleraldehyde elimination - Synergetic effect and byproducts
29 identification," *Chem. Eng. J.*, vol. 254, pp. 124–132, 2014.
30
- 31 [24] A. A. Assadi, A. Bouzaza, M. Lemasle, and D. Wolbert, "Removal of trimethylamine
32 and isovaleric acid from gas streams in a continuous flow surface discharge plasma
33 reactor," *Chem. Eng. Res. Des.*, vol. 93, no. May, pp. 640–651, 2014.
34
- 35 [25] A. A. Assadi, J. Palau, A. Bouzaza, and D. Wolbert, "Modeling of a continuous
36 photocatalytic reactor for isovaleraldehyde oxidation: Effect of different operating
37 parameters and chemical degradation pathway," *Chem. Eng. Res. Des.*, vol. 91, no. 7,
38 pp. 1307–1316, 2013.
39
- 40 [26] T. Zhu, Y. D. Wan, J. Li, X. W. He, D. Y. Xu, X. Q. Shu, W. J. Liang, and Y. Q. Jin,
41 "Volatile organic compounds decomposition using nonthermal plasma coupled with a
42 combination of catalysts," *Int. J. Environ. Sci. Technol.*, vol. 8, no. 3, pp. 621–630,
43 2011.

1
2
3
4
5
6
7
8
9
10
11
12
13
14
15
16
17
18
19
20
21
22
23
24
25
26
27
28
29
30
31
32
33

- [27] J. Van Durme, J. Dewulf, W. Sysmans, C. Leys, and H. Van Langenhove, "Efficient toluene abatement in indoor air by a plasma catalytic hybrid system," *Appl. Catal. B Environ.*, vol. 74, no. 1–2, pp. 161–169, 2007.
- [28] J. Van Durme, J. Dewulf, C. Leys, and H. Van Langenhove, "Combining non-thermal plasma with heterogeneous catalysis in waste gas treatment: A review," *Appl. Catal. B Environ.*, vol. 78, no. 3–4, pp. 324–333, 2008.
- [29] S. Li, Z. Ma, L. Wang, and J. Liu, "Influence of MnO₂ on the photocatalytic activity of P-25 TiO₂ in the degradation of methyl orange," *Sci. China, Ser. B Chem.*, vol. 51, no. 2, pp. 179–185, 2008.
- [30] Q. Jin, H. Arimoto, M. Fujishima, and H. Tada, "Manganese Oxide-Surface Modified Titanium(IV) Dioxide as Environmental Catalyst," *Catalysts*, vol. 3, no. 2, pp. 444–454, Apr. 2013.
- [31] F. Thevenet, L. Sivachandiran, O. Guaitella, C. Barakat, and a Rousseau, "Plasma-catalyst coupling for volatile organic compound removal and indoor air treatment: a review," *J. Phys. D. Appl. Phys.*, vol. 47, no. 22, p. 224011, 2014.
- [32] K. Allegraud. Décharge à Barrière Diélectrique de Surface : physique et procédé, thèse Ecole polytechnique de Paris, 2008.

1
2
3
4
5
6
7
8
9

10 **Figures:**

11 Figure 6. Sectional drawing and Schema of NTP coupled with catalysis in planar reactor.

12 Figure 7. Diagram of the impregnation technique for GFT synthesis "size press"

13 Figure 8. Variation of EC with inlet concentration at different flow rates ($SE = 17 \text{ J.L}^{-1}$, $T =$
14 20°C , $RH = 5\%$, $I = 20 \text{ W.m}^{-2}$).

15 Figure 9. Variation of EC with RH at different inlet concentrations ($SE = 17 \text{ J.L}^{-1}$, $Q_{\text{air}} = 2$
16 $\text{m}^3.\text{h}^{-1}$, $I = 20 \text{ W.m}^{-2}$).

17 Figure 5. Variation of conversion rate with relative humidity in function of different processes
18 using GFT with 100% TiO_2 ($Q_{\text{air}} = 2 \text{ Nm}^3.\text{h}^{-1}$, $[\text{C}_4\text{H}_8\text{O}] = 80 \text{ mg.Nm}^{-3}$, $E_{\text{inj}} = 17 \text{ J.L}^{-1}$, $RH = 5-$
19 7% , $T = 18-20^\circ\text{C}$).

20 Figure 6. By-products identified by GC-MS following butyraldehyde oxidation by the
21 combined system.

22 Figure 7. Suggested reaction scheme of BUTY oxidation by combination of GFT with 100%
23 TiO_2 and DBD.

1 Figure 8. CO₂ and CO selectivity's, and removal rate of oxidized butyraldehyde by
2 photocatalysis, plasma DBD and combined system ($Q_{\text{air}} = 2 \text{ Nm}^3 \cdot \text{h}^{-1}$, $[\text{C}_4\text{H}_8\text{O}] = 80 \text{ mg} \cdot \text{Nm}^{-3}$,
3 $E_{\text{inj}} = 12.8 \text{ J} \cdot \text{L}^{-1}$, RH = 5-7%, T = 18-20°C).

4 Figure 9. Effect of catalyst composition on BUTY conversion rate and the amount of formed
5 ozone by plasma-catalytic monobloc system (IPC) ($Q_{\text{air}} = 4 \text{ Nm}^3 \cdot \text{h}^{-1}$, $[\text{C}_4\text{H}_8\text{O}] = 50 \text{ mg} \cdot \text{Nm}^{-3}$,
6 $E_{\text{inj}} = 12.96 \text{ J} \cdot \text{L}^{-1}$, RH = 5-7 %, T = 18-20°C).

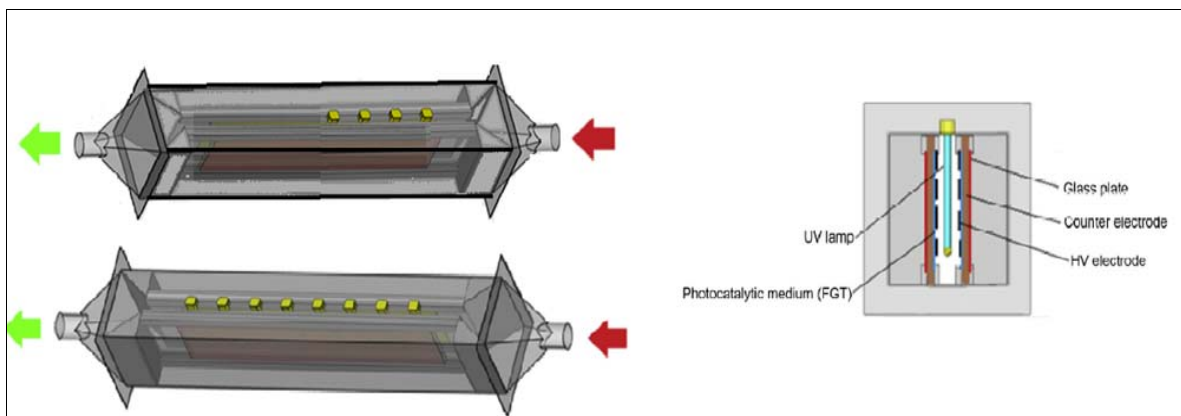
7 Figure 10. Comparison of the photocatalytic performance of different media for BUTY
8 oxidation ($Q_{\text{air}} = 4 \text{ Nm}^3 \cdot \text{h}^{-1}$, $[\text{C}_4\text{H}_8\text{O}] = 50 \text{ mg} \cdot \text{Nm}^{-3}$, RH = 5-7 %, T = 18-20°C)

9 Figure 11. Effect of RH on BUTY Conversion rate and ozone formation in PPC for the same
10 BUTY inlet concentration ($Q_{\text{air}} = 2 \text{ Nm}^3 \cdot \text{h}^{-1}$, $[\text{C}_4\text{H}_8\text{O}] = 50 \text{ mg} \cdot \text{Nm}^{-3}$, $E_{\text{inj}} = 12.96 \text{ J} \cdot \text{L}^{-1}$, T
11 = 18-20°C) On the left., RH = 5-7 %, On the right: RH = 55 %.

12

13

14



15

16 **Figure 10. Sectional drawing and Schema of NTP coupled with catalysis in planar reactor.**

17

18

19

20

21

22

1
2
3
4
5
6
7
8
9
10
11
12
13

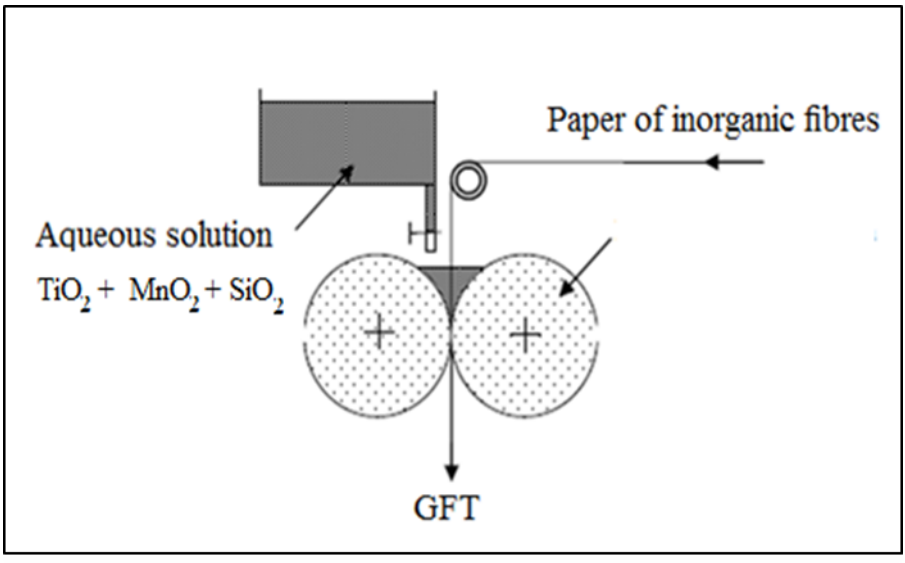
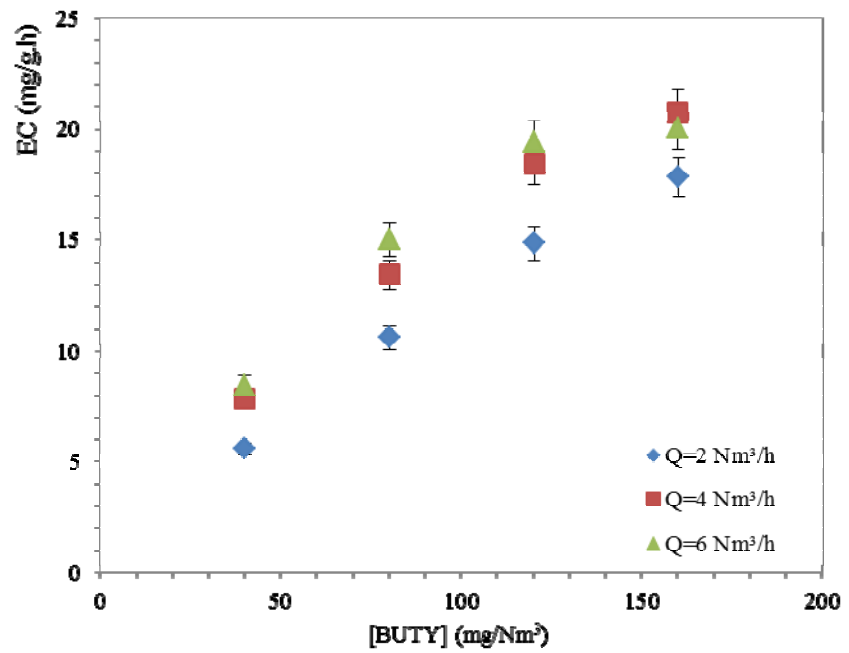


Figure 11. Diagram of the impregnation technique for GFT synthesis "size press"

14
15
16
17
18
19
20

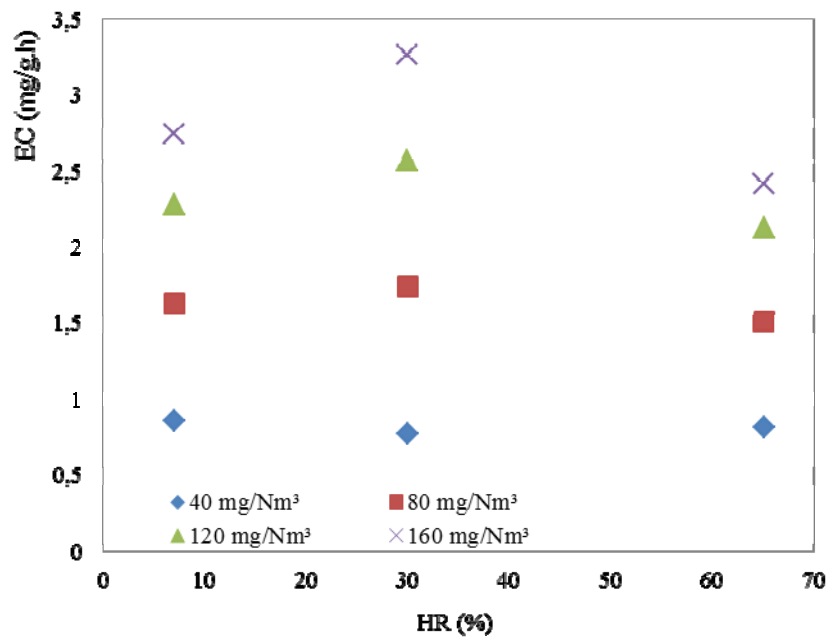
1
2
3
4
5
6
7
8
9
10
11
12
13
14
15



16
17
18
19

Figure 12. Variation of EC with inlet concentration at different flow rates (SE = 17 J.L⁻¹, T = 20°C, RH = 5%, I = 20 W.m⁻²).

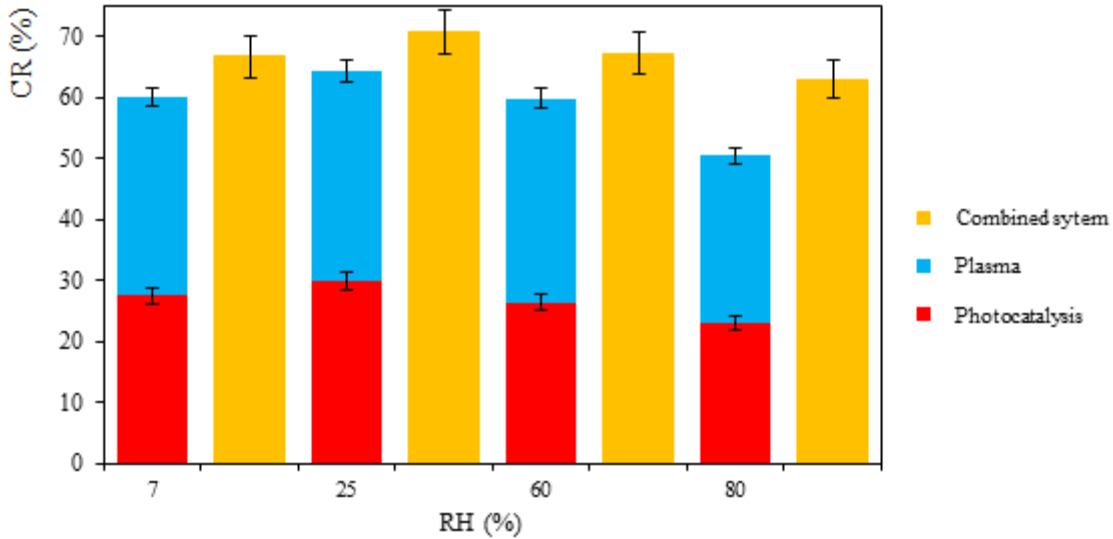
1
2
3
4
5
6
7
8
9
10
11
12
13
14



15
16
17
18

Figure 13. Variation of EC with RH at different inlet concentrations ($SE = 17 \text{ J.L}^{-1}$, $Q_{\text{air}} = 2 \text{ m}^3 \cdot \text{h}^{-1}$, $I = 20 \text{ W} \cdot \text{m}^{-2}$).

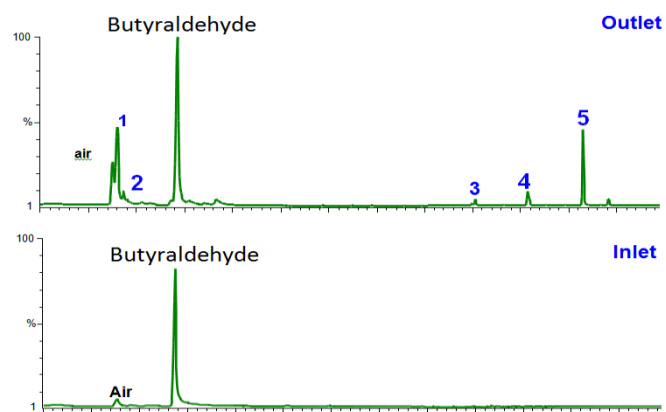
1
2
3
4
5
6
7
8
9
10
11
12
13
14



15
16
17
18
19
20

Figure 5. Variation of conversion rate with relative humidity in function of different processes using GFT with 100% TiO₂ ($Q_{air} = 2 \text{ Nm}^3 \cdot \text{h}^{-1}$, $[C_4H_8O] = 80 \text{ mg} \cdot \text{Nm}^{-3}$, $E_{inj} = 17 \text{ J} \cdot \text{L}^{-1}$, $RH = 5-7\%$, $T = 18-20^\circ\text{C}$).

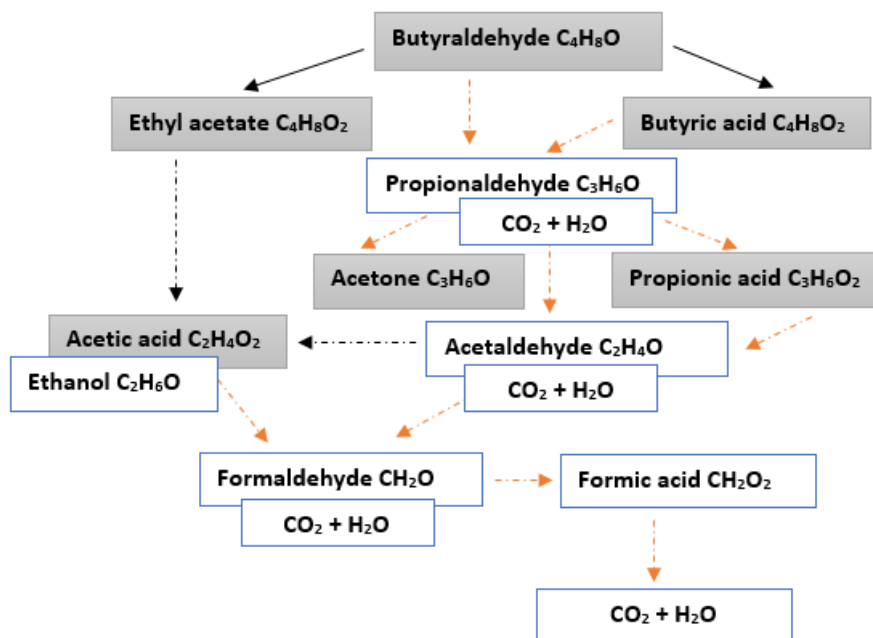
1
2
3
4
5
6
7
8
9
10
11
12
13
14
15



16
17
18
19
20
21
22

Figure 6. By-products identified by GC-MS following butyraldehyde oxidation by the combined system.

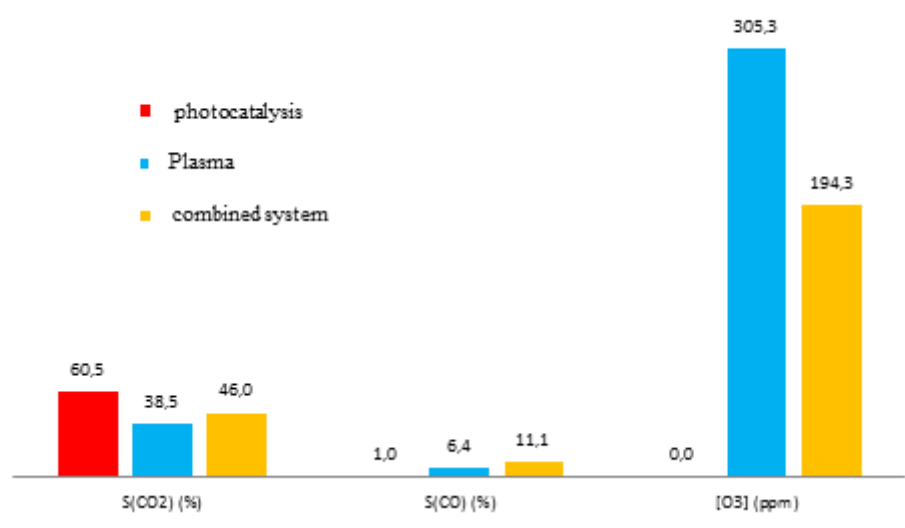
1
2
3
4
5
6
7
8
9
10
11
12
13
14



15
16
17
18

Figure 7. Suggested reaction scheme of BUTY oxidation by combination of GFT with 100% TiO₂ and DBD.

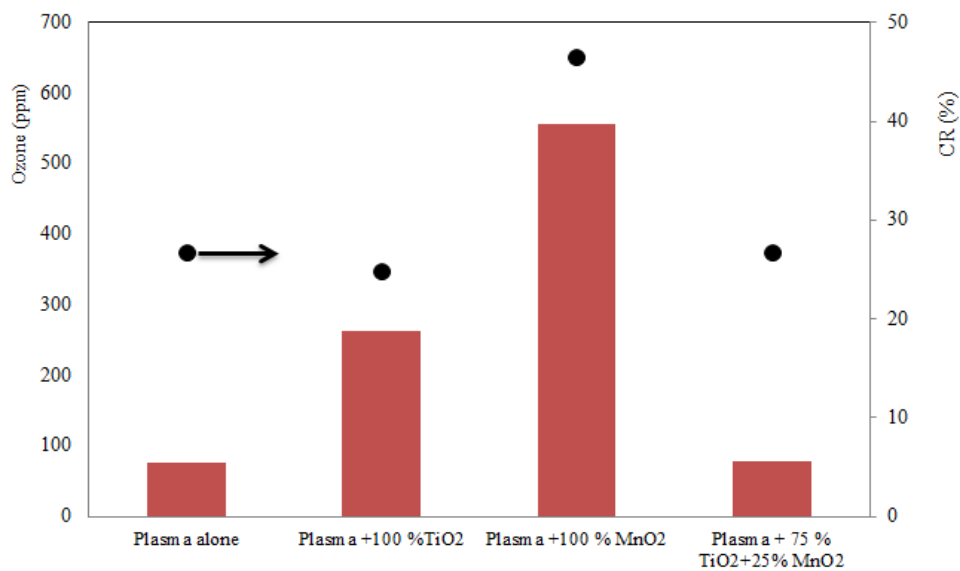
1
2
3
4
5
6
7
8
9
10
11
12
13
14



15
16
17
18
19
20

Figure 8. CO₂ and CO selectivity's, and removal rate of oxidized butyraldehyde by photocatalysis, plasma DBD and combined system ($Q_{\text{air}} = 2 \text{ Nm}^3 \cdot \text{h}^{-1}$, $[\text{C}_4\text{H}_8\text{O}] = 80 \text{ mg} \cdot \text{Nm}^{-3}$, $E_{\text{inj}} = 17 \text{ J} \cdot \text{L}^{-1}$, $\text{RH} = 5\text{-}7\%$, $T = 18\text{-}20^\circ\text{C}$).

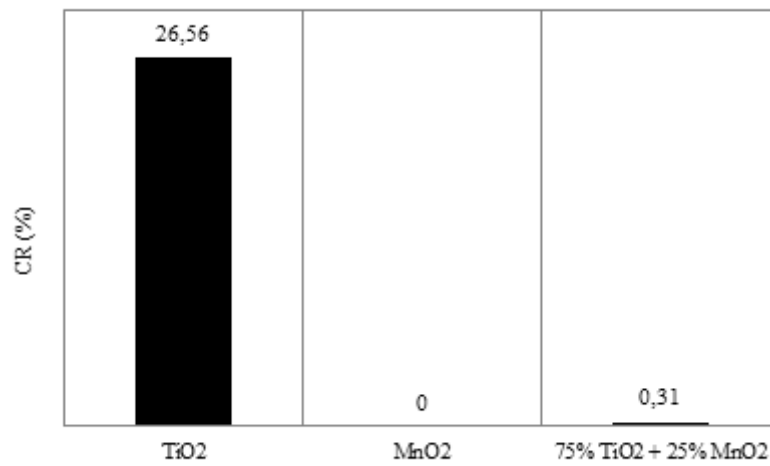
1
2
3
4
5
6
7
8
9
10
11
12
13
14



15
16
17
18
19
20

Figure 9. Effect of catalyst composition on BUTY conversion rate and the amount of formed ozone by plasma-catalytic monobloc system (IPC) ($Q_{\text{air}} = 4 \text{ Nm}^{-3} \cdot \text{h}^{-1}$, $[\text{C}_4\text{H}_8\text{O}] = 50 \text{ mg} \cdot \text{Nm}^{-3}$, $E_{\text{inj}} = 12.96 \text{ J} \cdot \text{L}^{-1}$, $\text{RH} = 5\text{-}7 \%$, $T = 18\text{-}20^\circ\text{C}$).

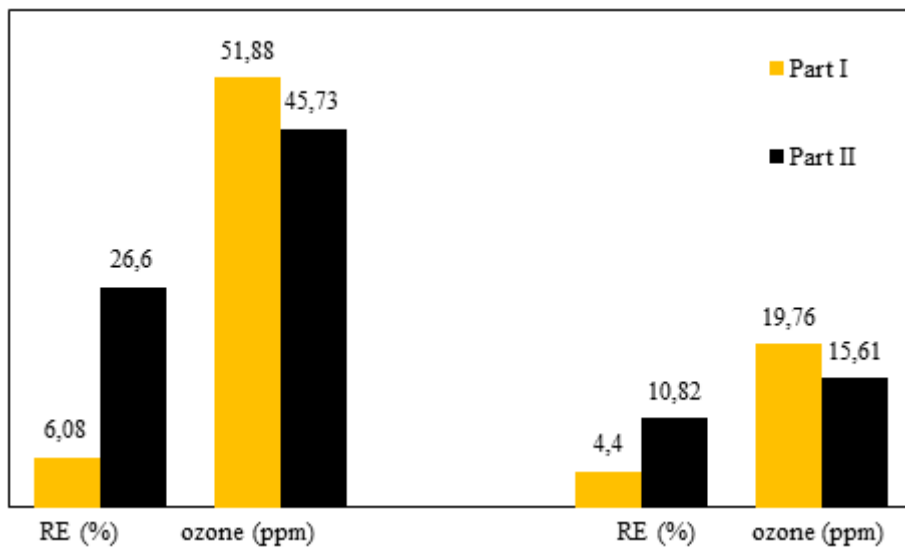
1
2
3
4
5
6
7
8
9
10
11
12
13
14



15
16
17
18
19
20

Figure 10. Comparison of the photocatalytic performance of different media for BUTY oxidation ($Q_{\text{air}} = 4 \text{ Nm}^{-3} \cdot \text{h}^{-1}$, $[\text{C}_4\text{H}_8\text{O}] = 50 \text{ mg} \cdot \text{Nm}^{-3}$, $\text{RH} = 5\text{-}7 \%$, $\text{T} = 18\text{-}20^\circ\text{C}$)

1
2
3
4
5
6
7
8
9
10
11
12
13
14
15
16
17



18
19
20
21

Figure 11. Effect of RH on BUTY conversion rate and ozone formation in PPC for the same BUTY inlet concentration ($Q_{\text{air}} = 2 \text{ Nm}^3 \cdot \text{h}^{-1}$, $[\text{C}_4\text{H}_8\text{O}] = 50 \text{ mg} \cdot \text{Nm}^{-3}$, $E_{\text{inj}} = 12.96 \text{ J} \cdot \text{L}^{-1}$, $T = 18\text{-}20^\circ\text{C}$) On the left: RH = 5-7 %, On the right: RH = 55 %.

